



## Modeling and assessment of adsorption ability of mussel powdered sunflower seed shell for Cr(VI) removal in batch and bed column systems

Amina Lahmar<sup>a</sup>, Sana Nouacer<sup>a</sup>, Ridha Djellabi<sup>b</sup>, Zhour Hattab<sup>a,\*</sup>, Yamina Berredjem<sup>c</sup>, Kamel Guerfi<sup>a</sup>

<sup>a</sup>Laboratory of Water Treatment and Valorization of Industrial Wastes, Department of Chemistry, Faculty of Sciences, Badji-Mokhtar University, B.P. 12, Annaba 23000, Algeria, emails: zoumourouda20012000@yahoo.fr (Z. Hattab), anima.lahmar@gmail.com (A. Lahmar), sanachimie@gmail.com (S. Nouacer), K\_guerfi@yahoo.fr (K. Guerfi)

<sup>b</sup>Università degli Studi di Milano, Dip. Chimica and INSTM-UdR Milano, Via Golgi, 19, 20133 Milano, Italy, email: ridha.djellabi@yahoo.com

<sup>c</sup>Science and Technology Laboratory of Water and Environment, Faculty of Science and Technology, Mohammed Cherif Messadia University, Souk Ahras 41000, Algeria, email: y\_berredjem@yahoo.fr

Received 4 October 2020; Accepted 21 March 2021

### ABSTRACT

The valorization of non-hazardous natural and industrial/agriculture wastes has got a lot of attention from the scientific and industrial communities as clean and alternative low-cost materials for environmental remediation. The present work aims to evaluate the sorption ability of valorized sunflower seed shells (SSS) for the recovery of toxic Cr(VI) in batch and bed column systems. The physicochemical features of SSS powdered material were checked using different techniques including scanning electron microscopy, Fourier-transform infrared, thermogravimetric analysis, and differential scanning calorimetry to better understand the Cr(VI) sorption behavior. Briefly, it was found that the surface of SSS is well-functionalized with amides, amines, and carboxylic groups, which in turn may induce strong surface interactions with Cr(VI) ions in the solution. Sorption experiments showed a total recovery of Cr(VI) at 10 ppm, temperature of 298 K, and pH 1 within 10 min. The regeneration of saturated SSS adsorbent was carried out by simple distilled water washing in the bed column system. The results showed that the Cr(VI) can be released from the surface of SSS, for possible reuse of the material. However, the adsorption efficiency was diminished slightly during recycling which might be due to the partial saturation of SSS surface with chemically bonded Cr(VI). The sorption kinetics in batch and column systems were evaluated using five models, and the mechanism for Cr(VI) sorption on SSS was discussed.

*Keywords:* Sunflower seed shell; Hexavalent chromium; Dynamic adsorption; Regeneration; Modeling

### 1. Introduction

Hexavalent chromium is one of the highly toxic heavy metals that can be found frequently in many industrial wastewaters due to the huge use of chromium reagents in the industry including metallurgy, electroplating, textile dyeing, and leather tanning.

Waters contaminated with Cr(VI) can lead to many human health diseases [1,2] and environmental perturbations.

The tolerance limit for chromium Cr(VI) in drinking water is set at 0.05 mg/L according to the World Health Organization [3].

In practice, there are several conventional methods used to remove hexavalent chromium in an aqueous solution, such as chemical/electrochemical precipitation [4], membrane filtration [5], adsorption [6], ion-exchange [7], coagulation/flocculation [8], and photocatalysis [9,10].

\* Corresponding author.

Among these, taking into consideration the factors of cost, efficiency, ease of use, regeneration capacity, adsorption is the most widely used technique for the removal of heavy metals from water [11]. The use of biomaterials as alternative adsorbents has received much attention in recent times. Although granular activated carbon is the most commonly used adsorbent for water treatment, it has been signaled to have certain limitations, such as costly chemical and thermal regeneration [12].

Different agricultural and lignocellulosic bioadsorbents have been the subject of previous studies because of their high adsorption capacity and low cost, such as egg-shell membrane [13], *Strychnos nux vomica* fruit shell [14], *Artocarpus heterophyllus* peel [15], olive pits [16], wood shaving [17]. As a result, the methodology adopted by using natural waste becomes rentable while at the same time contributing to sustainable development.

Based on the literature review, some of the research groups [18–20] have investigated the efficiency of SSS as an adsorbent for the removal of dyes. Other researchers have focused on the adsorption of heavy metals on SSS such as  $\text{Cu}^{2+}$ ,  $\text{Ni}^{2+}$ ,  $\text{Zn}^{2+}$ ,  $\text{Cd}^{2+}$ ,  $\text{Pb}^{2+}$ , etc. [21–27], also SSS was previously examined for removal of medicaments [28].

Since at a large scale, the sorption system can be carried out in different ways including batch and column processes, it would be better to evaluate the sorption ability of sunflower seed shell SSS as an alternative adsorbent in both systems. Therefore, in the present study, the adsorption kinetics of SSS toward the recovery of Cr(VI) from the water was evaluated in batch and column systems. The effects of operating parameters on the sorption performance were investigated.

Additionally, a numerical analysis is carried out and the experimental data were modeled using five models both in static and dynamic systems. The regeneration of SSS adsorbent was also studied in the column system.

## 2. Materials and methods

### 2.1. Chemicals

The set of chemicals used in adsorption tests such as sodium chloride (NaCl), hydrogen chloride (HCl), sodium hydroxide (NaOH), sulfuric acid ( $\text{H}_2\text{SO}_4$ ), 1,5-diphenylcarbazine, and potassium dichromate ( $\text{K}_2\text{Cr}_2\text{O}_7$ ) were purchased from Sigma-Aldrich-Fluka (Saint-Quentin, Fallavier, France).

### 2.2. Preparation of SSS

Sunflower seed husks were collected from the local market. To remove impurities, the material was washed several times with water and then with distilled water. Afterwards, in an electric mill, the SSS were crushed and then sieved with an Afnor sieve. Only particles with a diameter smaller than 315  $\mu\text{m}$  were used for the experimental adsorption tests.

### 2.3. Characterization of SSS

The morphology of SSS was determined by scanning electron microscopy (SEM) using (Quanta 200 FEI) combined

with energy-dispersive X-ray. Functional groups were identified by FTIR using IR<sup>-1</sup> affinity in combination with a single ATR reflection. Thermogravimetric analysis (TGA) and differential scanning calorimetry (DSC) was carried out on METTLER TOLEDO STARe TGA/DSC 3+ System (Greifensee, Switzerland), at a heating rate from 10°C/min (30 mL/min) up to 600°C under  $\text{N}_2$  flow gas atmosphere.

## 3. Batch adsorption

The adsorption experiments were carried out in a batch process, a dose of SSS 12.5 g/L was used in all the experiments and was mixed with 250 mL of synthetic Cr(VI) solution of desired concentration in 500 mL beakers. The effect of various process parameters on the efficiency of Cr(VI) removal was investigated by varying different parameters such as pH (1–6), initial Cr(VI) concentration (10–30 mg/L), and temperature (25°C–45°C). Continuous mixing was provided during the experiments with 30 min contact time at constant agitation 50 rpm. After adsorption equilibrium, the mixture was filtered and residual Cr(VI) concentration was determined by UV/Vis absorption spectrophotometer (Jenway 7315) at 545 nm by complexing Cr(VI) with 1,5-diphenylcarbazine.

The adsorption capacity  $q_e$  (mg/g) of SSS was calculated by Zohra et al. [29]:

$$q_e = \frac{(C_0 - C_e) \cdot V}{m} \quad (1)$$

where  $C_0$  and  $C_e$  are the initial and equilibrium concentrations (mg/L), respectively, of pollutant in solution,  $V$  is the volume of the solution (L), and  $m$  is the weight (g) of the adsorbent.

The removal rate  $R(\%)$  of SSS was calculated by:

$$R = \frac{C_0 - C_e}{C_0} \times 100 \quad (2)$$

### 3.1. Batch adsorption isotherms

Five theoretical models were applied in this study: Langmuir [30], Freundlich [31], Temkin [32], Redlich-Peterson [33], and Sips [34].

#### 3.1.1. Langmuir isotherm

According to Langmuir [30] model, the surface of adsorbent is considered to be homogenous, forming a monolayer with the adsorbate through constant heat of adsorption for all sites without interaction between adsorbed molecules. The Langmuir model Eq. (3) is given below:

$$q_e = \frac{q_m K_L C_e}{1 + K_L C_e} \quad (3)$$

Eq. (3) can be linearized to:

$$\frac{1}{q_e} = \frac{1}{q_m} + \frac{1}{q_m K_L} \left( \frac{1}{C_e} \right) \quad (4)$$

where  $q_e$  is the amount of Cr(VI) adsorbed per gram of the adsorbent at the equilibrium (mg/g),  $q_m$  is the maximum monolayer coverage capacity (mg/g),  $C_e$  is the equilibrium concentration of adsorbate (mg/L) and  $K_L$  is the Langmuir constant. The values of  $q_{\max}$  and  $K_L$  were calculated from the slope and intercept of the Langmuir plot of  $1/C_e$  vs.  $1/q_e$ .

### 3.1.2. Freundlich isotherm

The Freundlich [31] model, suggested that the removal of adsorbent occurs on heterogenous adsorbant surface, and can be applied to multilayer adsorption. These data regularly fit the empirical equation suggested by Freundlich:

$$q_e = K_F C_e^{1/n} \quad (5)$$

Eq. (5) can be shifted to obtain the linear form by taking logarithms:

$$\log q_e = \log K_F + \frac{1}{n} \log C_e \quad (6)$$

where  $q_e$  is the quantity of Cr(VI) adsorbed mg/g,  $C_e$  is the equilibrium concentration of adsorbate mg/L.  $K_F$  (mg/L) is the Freundlich isotherm constant and  $n$  is a relative factor of adsorption intensity, it can be also named a heterogeneity factor.  $K_F$  and  $1/n$  can be calculated from intercept and the slope of the linear plot  $\log C_e$  and  $\log q_e$ .

### 3.1.3. Temkin isotherm

This model describes the interaction between adsorbent–adsorbate. It assumes that a linear variation of the adsorption heat with the degree of overlap [32]. The Temkin model isotherm is described by (7):

$$q_e = \frac{RT}{b_T} \ln A_T C_e \quad (7)$$

Eq. (7) can be rearranged as:

$$q_e = B \ln A_T + B \ln C_e \quad (8)$$

where  $B = RT/b_T$  and is related to the heat of adsorption,  $T$  (K) is absolute temperature,  $R$  implies the universal gas constant (8.314 J/K mol),  $b_T$  (J/mol) is the Temkin isotherm constant, and  $A$  (L/mg) is the equilibrium binding constant.

### 3.1.4. Sips isotherm

Sips [34] combined the Langmuir and the Freundlich isotherms. The model has been used in the following nonlinear Eq. (9):

$$q_e = \frac{q_{\max} K_S C_e^{1/n}}{1 + K_S C_e^{1/n}} \quad (9)$$

Eq. (9) can be linearized:

$$\log \left( \frac{q_e}{q_{\max} - q_e} \right) = \frac{1}{n} \log C_e + \log K_S \quad (10)$$

where  $K_S$  is the sips constant related with affinity ( $\text{mg}^{1/n}/\text{L}^{1/n}$ ) and  $q_{\max}$  is the maximum adsorption capacity (mg/g).

### 3.1.5. Redlich–Peterson isotherm

This model is also a combination of both Langmuir and Freundlich models equations. It is given by Eq. (11) below:

$$\log \frac{C}{q_e} = \beta \log C_e - \log A \quad (11)$$

where  $A$  is the Redlich–Peterson constant,  $\beta$  is the exponent and its value lies between 0 and 1. If the value of  $\beta$  is close to 1, it defines Langmuir adsorption and if  $\beta$  is close to 0, Freundlich is the predominant isotherm [35,36]

## 4. Column adsorption

The adsorption tests have been carried out in a glass column with 11 mm in diameter. The residual Cr(VI) concentration was determined at a wavelength of  $\lambda_{\max} = 545$  nm using UV-Vis spectrophotometer (JENWAY 7315) after complexation with 1,5-diphenylcarbazide according to the method described by Jean Rodier [37].

Different quantities of SSS, 0.17, 0.33, and 0.50 g corresponding to bed heights of 10, 20, and 30 mm, respectively, were used.

The adsorption profile of sorbate in a fixed-bed column results in an S-shaped curve called breakthrough curve [38]. Breakthrough curves profiles of Cr(VI) adsorption were obtained from  $C_t/C_0$  as a function of flow time [39]. The breakthrough time  $t_b$  are defined when  $C_t/C_0 = 0.1$  and exhaustion time  $t_e$  when  $C_t/C_0 = 0.98$ .

The set of equations used in this work are summarized in Table 1.

### 4.1. Models and kinetic tests of fixed-bed column adsorption

Five theoretical models were applied in this study: Thomas, Yoon and Nelson, Bohart–Adams, Wolborska and BDST.

#### 4.1.1. Thomas model

Thomas model are applied to the progress of biosorption in the absence of external and internal diffusion limitations [44]. It is employed to calculate the adsorption rate constant and the concentration in the solid phase of adsorbate on the adsorbent from the fixed bed studies, this model is represented in Table 2.

#### 4.1.2. Yoon and Nelson model

Yoon and Nelson developed a simple model of adsorption (penetration) of vapor in the adsorbate that

Table 1  
Equations used for fixed bed analyses

Volume of treated effluent	$V_{\text{eff}} = F(t_c)$	(12)	[40]
Total amount of Cr(VI) adsorbed	$Q_{\text{total}} = \frac{F}{1,000} A$ $= \frac{F}{1,000} \int_t^{t=\text{total}} C_{\text{ads}} dt$	(13)	[41]
Experimental absorption amount	$Q_{\text{exp}} = \frac{Q_{\text{total}}}{m}$	(14)	[42]
Maximum adsorption capacity	$N_{\text{exp}} = Q_{\text{exp}} \frac{m}{V}$	(15)	[13]
Quantities of adsorbate passed in the column	$W_{\text{total}} = \frac{C_0 Q_{\text{total}}}{1000}$	(16)	[40]
Removal rate	$R\% = \frac{Q_{\text{total}}}{W_{\text{total}}} \times 100$	(17)	[43]

Table 2  
Five models used for fixed bed analyses

Model of Thomas	$\frac{C_t}{C_0} = \frac{1}{1 + \exp\left(\frac{K_{\text{th}} m q_{\text{th}}}{U} - C_0 K_{\text{th}} t\right)}$	(18)	[44]
Model of Yoon–Nelson	$\frac{C_t}{C_0} = \frac{1}{1 + e^{K_{\text{YN}}(\tau-t)}}$	(19)	[45]
Model of Bohart–Adams	$\frac{C_t}{C_0} = \exp\left(K_{\text{BA}} C_0 t - K_{\text{BA}} N_0 \frac{Z}{U}\right)$	(20)	[46]
Model of Wolborska	$\frac{C_t}{C_0} = \exp\left(\frac{\beta_a C_0}{N_0} t - \frac{\beta_a Z}{U}\right)$	(21)	[47]
Model of BDST	$t_b = \frac{N'_0}{C_0 U} Z - \frac{1}{K_{\text{BA}} C_0} \ln\left(\frac{C_0}{C_b} - 1\right)$	(22)	[46]

was gas on activated carbon. This model has founded on the hypothesis that the rate of decrease in the probability of adsorption for every adsorbate molecule was proportional to the probability of the adsorbate penetrating on the adsorbent and the probability of breakthrough of the adsorbate on the adsorbent. Yoon and Nelson’s model is less complex than the other models as it does not need detailed data on the type of adsorbent, the physical properties of the adsorption bed, and the characteristics of the adsorbent [45], this model is represented in Table 2

#### 4.1.3. Bohart–Adams model

Bohart–Adams model is used to describe the first section of the breakthrough curve, even though the original work by Bohart–Adams was carried out for the gas–coal adsorption system, his global approach can also be applied in the quantitative description of other systems. The Bohart–Adams model supposes that adsorption efficiency is proportional to both the residual capacity of the activated carbon and the concentration of the adsorbent species [46], this model is represented in Table 2.

#### 4.1.4. Wolborska model

Wolborska model is based on the general mass transfer equations for the diffusion mechanism in the range of the low-concentration breakthrough curve. This model can be employed for experimental data describing the first part of the breakthrough curve [47], the model is represented in Table 2.

#### 4.1.5. BDST model

The bed depth service time model was originally suggested by Bohart and Adams [46] in 1920. It supposes that the adsorption efficiency is controlled by the surface reaction between the unused capacity of the adsorbent and the adsorbate. It is used for estimating the bed depth necessary for a given operating time. A linear relationship between bed depth and operating time is given by the equation in Table 2.

## 5. Results and discussion

### 5.1. Characterization of SSS

#### 5.1.1. SEM analysis

Fig. 1 represents SEM images of sunflower seed shells at different enlargements. The micrographs clearly reveal that the wall of a cell has a significant number of small holes; these holes promote the transport of chemical species in all directions through the shell (diffusion phenomenon) which may be suitable for the retention of pollutants [48].

#### 5.1.2. FTIR and EDX analysis

Fig. 2 shows the FTIR spectrum for SSS. Different peaks were detected which are attributed to various functional groups and bands.

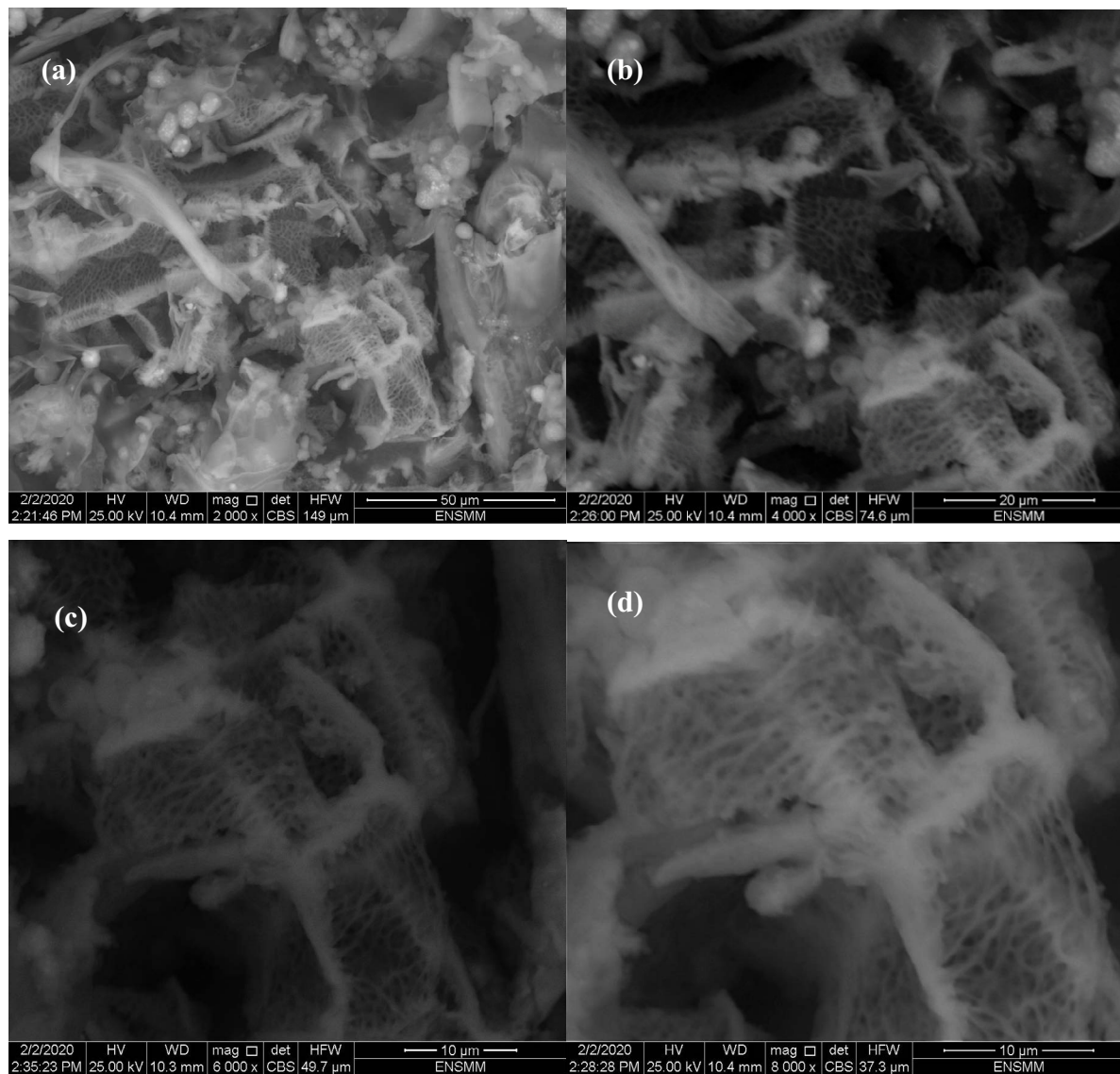


Fig. 1. SEM images of SSS (a) X2000, (b) X4000, (c) X6000, and (d) X8000 before Cr(VI) adsorption.

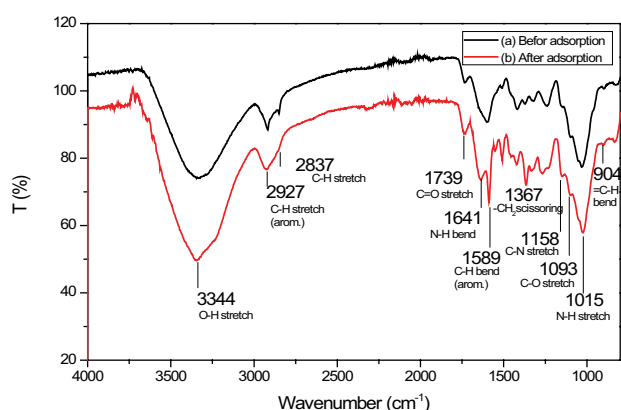


Fig. 2. FTIR spectra (a) before and (b) after Cr(VI) adsorption.

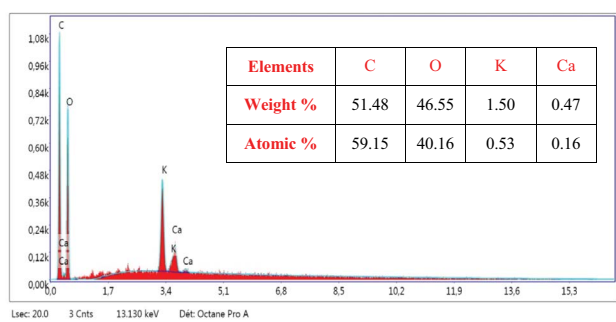


Fig. 3. EDX profile of SSS before adsorption.

Sunflower shells are lignocellulosic materials with a chemical composition consisting of hemicelluloses, lignin, and celluloses. The band at  $3,352\text{ cm}^{-1}$  is assigned to N–H and –OH stretching mode. Bands at  $2,940$ ,  $2,862\text{ cm}^{-1}$  are attributed to C–H of aromatic components and C–H stretching vibration. The peak at  $1,747\text{ cm}^{-1}$  is due to C=O carboxyl or ester groups and  $1,629\text{ cm}^{-1}$  of N–H amide bonding. The absorption peak appears at around  $1,617\text{ cm}^{-1}$  is attributed to aromatic ring vibrations of lignin and  $1,114\text{ cm}^{-1}$  is attributed to –C–O alcohols and carboxylic acids. Bands at  $1,388$  and  $1,173\text{ cm}^{-1}$  are due to  $\text{CH}_2$  scissoring and C–N amine stretching respectively [18,19,49].

On the other hand, after Cr(VI) adsorption, the following changes occurred a decrease in the intensity and a slight shift in the position of some peaks for instance –OH and N–H:  $3,344\text{ cm}^{-1}$ , C=O:  $1,739\text{ cm}^{-1}$ , and amine C–N:  $1,158\text{ cm}^{-1}$ . The observed changes signify that an interaction occurred between the Cr(VI) and SFS particles surface. As shown in Fig. 3, the highest values of carbon and oxygen indicate the organic nature of the adsorbent [50].

### 5.1.3. Thermogravimetric analysis

A chemical substance subjected to thermal treatment may undergo changes in its physico-chemical properties such as phase change, volume change, decomposition, structural alteration, etc. [51].

Five distinct stages can be identified that are associated with the thermal destruction and oxidation of biomass

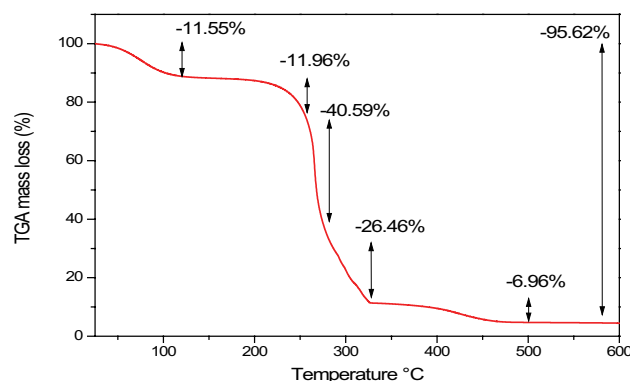


Fig. 4. TGA analysis.

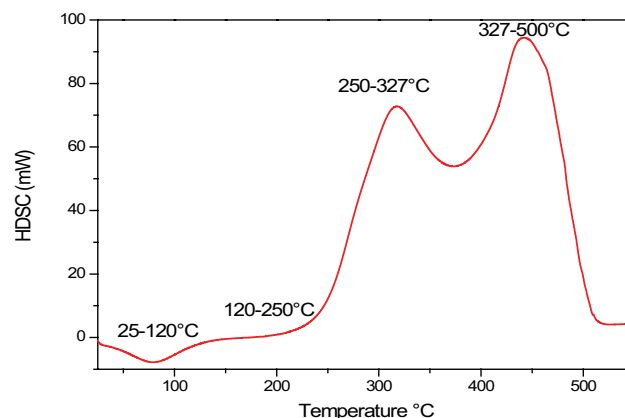


Fig. 5. DSC analysis.

particles in Fig. 4 The first stage  $25\text{ °C}–120\text{ °C}$  corresponds to the loss of about 11.55% of the sample weight due to the dehydration of the sample [52]. The second weight loss is 11.96% in the temperature range of  $120\text{ °C}–250\text{ °C}$  which corresponds to the depolymerization of hemicellulose. The third stage  $250\text{ °C}–327\text{ °C}$  with the highest loss of 40.59%, it indicates the degradation of celluloses [53], the fourth stage  $327\text{ °C}–500\text{ °C}$  with the loss of 26.46%, corresponds to the degradation of the lignin and the fifth stage  $500\text{ °C}–600\text{ °C}$  correspond to carbonaceous residues 6.96% [54].

### 5.1.4. DSC analysis

The results of DSC analysis in Fig. 5 illustrate that there are different exothermic peaks produced, confirming the different weight losses identified in the TGA analysis [55].

Two important exothermic thermal effects were observed on the DSC curves, which could be due to the decomposition of hemicellulose, cellulose, and lignin [56].

The first stage  $25\text{ °C}–120\text{ °C}$  corresponds to the loss of the sample weight due to the dehydration of the sample [52]. The second weight loss in the temperature range of  $120\text{ °C}–250\text{ °C}$  that corresponds to the depolymerization of hemicellulose. the third stage  $250\text{ °C}–327\text{ °C}$  with the highest loss, indicates the degradation of celluloses [53], the fourth stage  $327\text{ °C}–500\text{ °C}$  corresponds to the degradation of the lignin.

## 5.2. Batch results

### 5.2.1. Effect of pH

The pH of the solution is an important parameter for the adsorption process of metallic ions. It can change the ionization of the adsorbent surface and the metallic cation species in the aqueous solution. Moreover, it can also affect the biosorption mechanism of different ions on the biomaterial surface. The effect of the initial pH of the solution on the chromium adsorption by SSS was studied by varying the pH from 1 to 6, the results are illustrated in Fig. 6. From these results, it is clear that the Cr(VI) depends strongly on the pH. The adsorption efficiency decrease with the increase of pH and the maximum capacity adsorption was found at the pH = 1, where the predominant form of Cr(VI) is  $\text{HCrO}_4^-$ . This behavior is explained by the role which has the acidic pH, the functional groups present in the SSS surface undergo a strong protonation which gives the material a global positive charge. The  $\text{pH}_{\text{zpc}}$  value is in accord with the free pH and the total acidity of the biomaterial. The same result is obtained with SSS at a fixed-bed column study.

### 5.2.2. Effect of initial concentration of Cr(VI) and contact time

The biosorption process depends considerably on initial concentration to access the reaction kinetics. In order to find out the equilibrium contact time, the experiment was carried out for 30 min of Cr(VI) adsorption at different initial concentration from 10 to 30 mg/L. The results in Fig. 7 indicate that the fixation of Cr(VI) on SSS was very fleetly at the first 5 min after that, a stationary phase is attained. An increase in the adsorption capacity was observed from 0.7 to 2.8 mg/g when the initial concentration of Cr(VI) expand from 10 to 30 mg/L. Such behavior is established by the availability of several adsorption sites on the SSS surface in the initial phase of the reaction, which becomes progressively saturated of Cr(VI) with increasing contact time. Zohra et al. [29] reported that the rapid initial phase can be related to physical adsorption or ion exchange at

the surface and the subsequent stationary phase may be due to other mechanisms like aggregation, micro-precipitation, or saturation of binding sites.

### 5.2.3. Effect of temperature

Effect of temperature on the adsorption capacity of Cr(VI) at 20°C, 30°C, and 40°C by SSS was studied at pH = 1, chromium concentration 10 ppm, and dose adsorbent 12.5 g/L. As shown in Fig. 8 the temperature has no effect on the capacity adsorption of Cr(VI) on SSS. However, there is no significant decrease in the capacity absorption average of 3% when the temperature increases from 20°C to 40°C. This compartment can be due to the partial deactivation of the SSS surface or it can be explained by the destruction of some active sites by destroying their surface bonding. A similar result was found by other researchers [57,58].

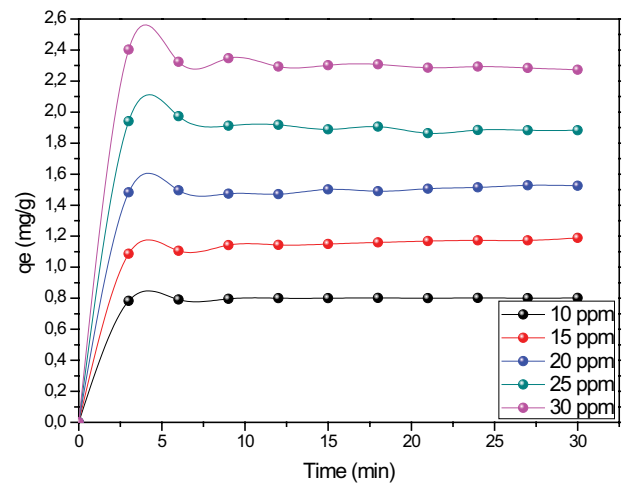


Fig. 7. Influence of Cr(VI) concentration on adsorption capacity.

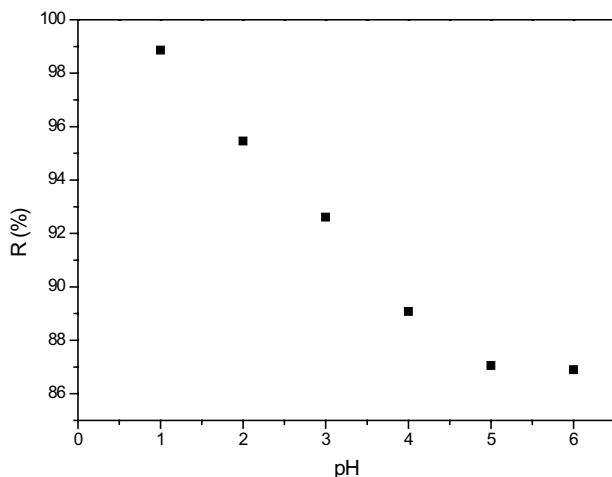


Fig. 6. Effect of pH on Cr(VI) adsorption.

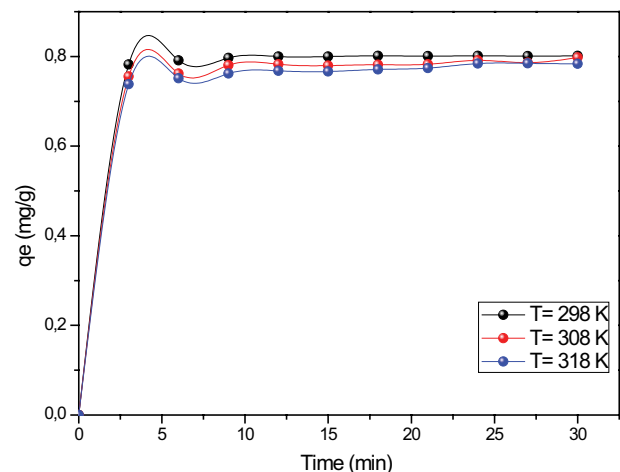


Fig. 8. Influence of temperature on Cr(VI) adsorption.

5.2.4. Batch modeling

The modeling adsorption was carried out from experimental results by varying temperature (20°C, 30°C, and 40°C), initial concentration of Cr(VI) 10 mg/L for 30 min contact time at pH = 1. The plot of linearized of Langmuir (a), Freundlich (b), Sips (c), Temkin (d), and Redlich–Peterson are illustrated in Fig. 9, the calculated isotherms parameters are given in Table 3.

From the Table 3, Langmuir model presents better experimental data as compared to other models. This was attributed to the higher value of the correlation coefficient ( $R^2$ ) and the maximum capacity adsorption is in agreement with the experimental value. All these results confirmed that

the adsorption is a monolayer. The value of  $B-0$  in the Temkin isotherm model showed that the adsorption is a thermal [59], in addition the value of  $B$  in the Redlich–Peterson model are close to 1 and also it favored the Langmuir model.

5.3. Dynamic sorption

5.3.1. Effect of flow rate

From Fig. 10 and Table 3, a high flow rate results in a reduction in operating time and a decrease in the percentage of Cr(VI) removal. This can be explained by the fact that by increasing the flow rate, the flux of the pollutant increases, resulting in insufficient contact time for mass transfer

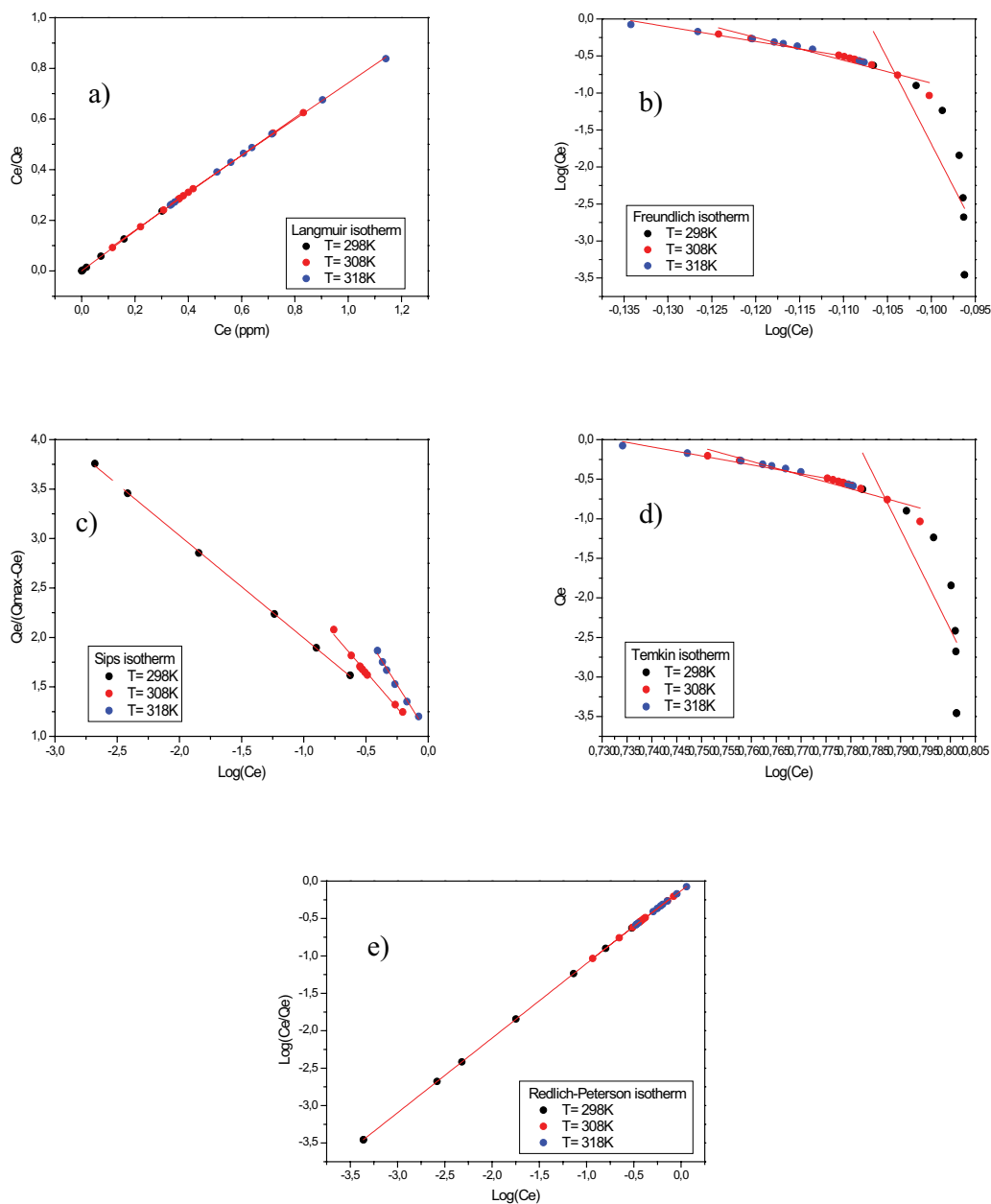


Fig. 9. Isotherm models of (a) Langmuir, (b) Freundlich, (c) Sips, (d) Temkin, and (e) Redlich–Peterson.

Table 3  
 Constants of isotherm models for Cr(VI) adsorption on SSS

Isotherm models	Parameters	20°C	30°C	40°C
Langmuir	$K_L$ (L/mg)	1	64.33	29.48
	$q_{\max}$ (mg/g)	1.27	1.34	1.39
	$R^2$	1	0.9997	0.9996
Freundlich	$K_f$	0.78	0.75	0.73
	$1/n$	-0.0027	-0.0289	-0.0486
	$R^2$	0.6249	0.8896	0.9601
Temkin	$A_T$ (L/g)	0	$2.88 \times 10^{-15}$	$2.39 \times 10^{-9}$
	$B$	-0.0049	-0.0514	-0.0850
	$R^2$	0.6145	0.8949	0.9639
Sips	$K_s$ (mg/L) <sup>-1/n</sup>	9.05	8.38	10.57
	$n_s$	-0.96	-0.68	-0.24
	$R^2$	0.9997	0.9909	0.9916
Redlich–Peterson	$\beta$	0.9872	1.0289	1.0289
	$A$ (L/g)	-1.16	-1.34	-1.36
	$R^2$	0.9994	0.9999	0.9999

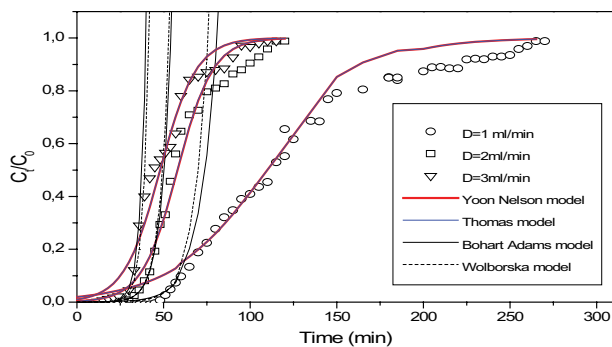


Fig. 10. Comparison of theoretical and experimental penetration curves at different flow rates according to the models studied for Cr(VI) adsorption by SSS ( $Z = 20$  mm,  $C_0 = 10$  mg/L,  $\text{pH} = 1 \pm 0.1$ , and  $T = 298$  K).

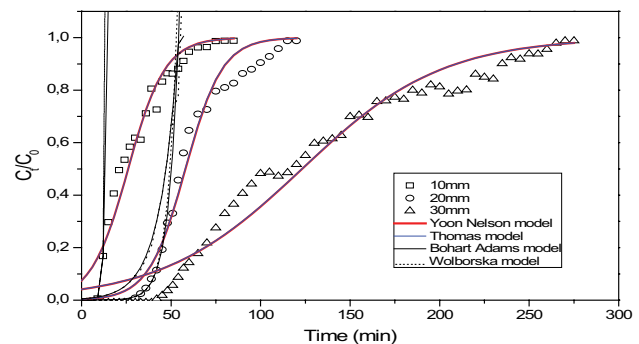


Fig. 11. Comparison of theoretical and experimental penetration curves at different bed height according to the models studied for Cr(VI) adsorption by SSS ( $F = 2$  mL/min,  $C_0 = 10$  mg/L,  $\text{pH} = 1 \pm 0.1$ , and  $T = 298$  K).

between the adsorbate and the bioadsorbent, diffusion of the pollutant into the pores of the adsorbent, and a limited number of active sites and ionic biomass groups for matrix biosorption [13].

### 5.3.2. Effect of bed height

The mass of the adsorbent is proportional to the height of the bed, this means that an increase in bed height increases the mass of the adsorbent, and thus the number of sorption sites increases, which in turn increases the sorption capacity (Fig. 11 and Table 4) [60].

### 5.3.3. Effect of initial concentration

As shown in Fig. 12, by decreasing the initial Cr(VI) concentration, the breakthrough curves occurred later, and the volume of the column outlet was higher, resulting in a higher breakthrough time. This means that at a low initial

concentration of Cr(VI), a lower concentration gradient leads to a decrease in the diffusion coefficient, which in turn slows down the transport of the pollutant in the pores of the adsorbent.

Whereas, at a higher initial Cr(VI) concentration, the SSS gets saturated quickly because the binding sites are more rapidly saturated in the column, allowing for earlier breakthrough and exhaustion time. A decrease in the percentage of removal with a higher Cr(VI) concentration indicates that adsorption is dependent on the availability of binding sites [61].

### 5.3.4. Effect of pH

Depending on the pH, Cr(VI) is found in different ionic forms in the water. In the range of pH studied  $\text{pH} = 1, 2,$  and  $3$ , the  $\text{HCrO}_4^-$  is the predominant species of Cr(VI) [62]. By studying the effect of pH in this range, it was found that the adsorption capacity increases with decreasing pH, this

Table 4  
Conditions and results for fixed-column experiments

$C_0$ (mg/L)	$Z$ (mm)	$F$ (mL/min)	pH	$T$ (K)	$t_b$ (min)	$t_{total}$ (min)	$V_{eff}$ (mL)	$W_{total}$ (mg)	$q_{total}$ (mg)	$q_{exp}$ (mg/g)	$R$ (%)
10	10	2	1	298	12	80	160	1.14	0.58	3.42	51.11
10	20	2	1	298	42	115	230	2.10	1.26	3.84	60.47
10	30	2	1	298	57	235	470	4.60	3.04	6.08	66.10
5	20	2	1	298	57	192	384	1.47	0.93	2.84	63.83
15	20	2	1	298	21	120	240	2.55	1.32	4.00	51.85
10	20	1	1	298	65	265	265	2.20	1.34	4.08	61.34
10	20	3	1	298	33	105	115	2.70	1.56	4.74	57.96
10	20	2	2	298	4	51	102	1.02	0.40	1.23	40.02
10	20	2	3	298	0	50	100	0.3	0.08	0.26	29.28
10	20	2	1	318	30	180	360	2.90	1.34	4.07	46.33
10	20	2	1	308	36	240	480	4.10	2.05	6.22	50.08

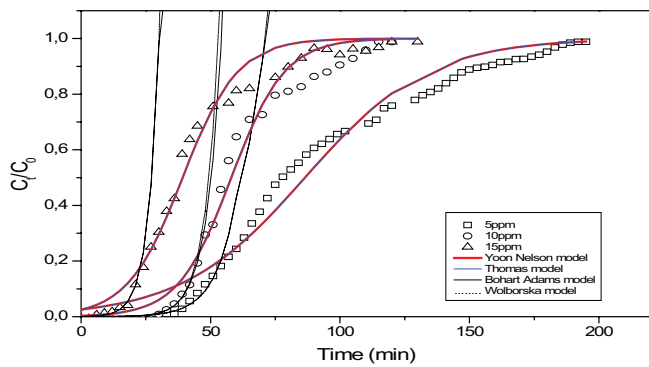


Fig. 12. Comparison of theoretical and experimental penetration curves at different Cr(VI) concentrations according to the models studied for Cr(VI) adsorption by SSS ( $F = 2$  mL/min,  $Z = 20$  mm,  $pH = 1 \pm 0.1$ , and  $T = 298$  K).

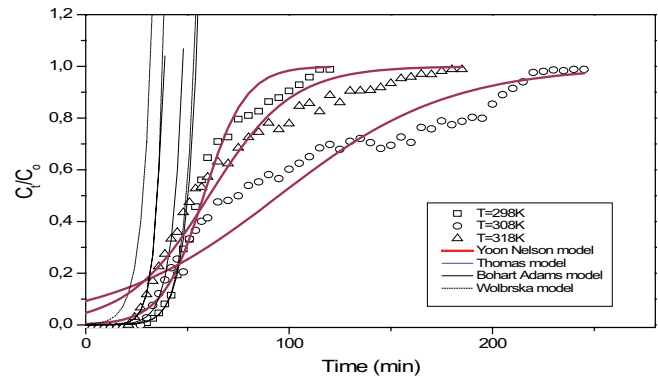


Fig. 14. Comparison of theoretical and experimental penetration curves at different temperature according to the models studied for Cr(VI) adsorption by SSS ( $F = 2$  mL/min,  $Z = 20$  mm,  $C_0 = 10$  mg/L, and  $pH = 1 \pm 0.1$ ).

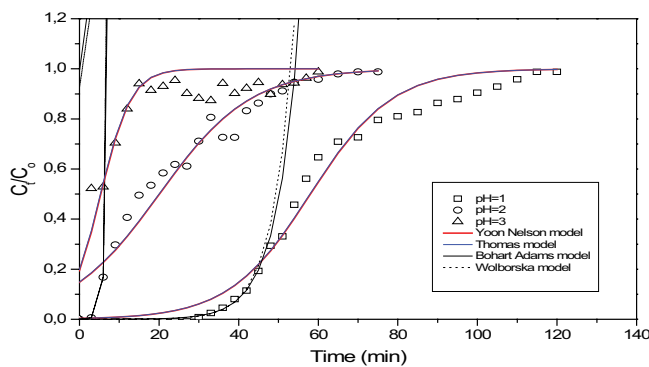


Fig. 13. Comparison of theoretical and experimental penetration curves at different pH according to the models studied for Cr(VI) adsorption by SSS ( $F = 2$  mL/min,  $Z = 20$  mm,  $C_0 = 10$  mg/L, and  $T = 298$  K).

can be explained by the fact that at a lower pH, there is an increase in the number of proton  $H^+$  on the adsorbent surface which leads to a significantly strong electrostatic attraction between the positively charged adsorbent surface and the

negatively charged chromate ions [63]. The results are shown in Fig. 13 and listed in Table 4.

### 5.3.5. Effect of temperature

As can be seen in Table 4 and Fig. 14, the increase in temperature leads to a decrease in exhaustion time and efficiency rate, revealing an exothermic process.

A variation in temperature has no significant effect on the adsorption capacity, this result is in agreement with the results found in the batch study. 298 K was therefore chosen as the optimal temperature for further studies.

### 5.3.6. Regeneration of SSS

Desorption of Cr(VI) molecules adsorbed in the SSS bed column was realized by washing with distilled water. The SSS showed satisfactory performance in removing Cr(VI) from the solution during the ninth adsorption–desorption cycles as can be seen in Figs. 15 and 16. The adsorption capacity for Cr(VI) was reduced after each

cycle was used. The decrease in removal efficiency can be assigned to the loss of partial reduction property of SFS during adsorption–desorption processes. The adsorption efficiency decreased from 60.47% to 56.91% after the tenth adsorption [64].

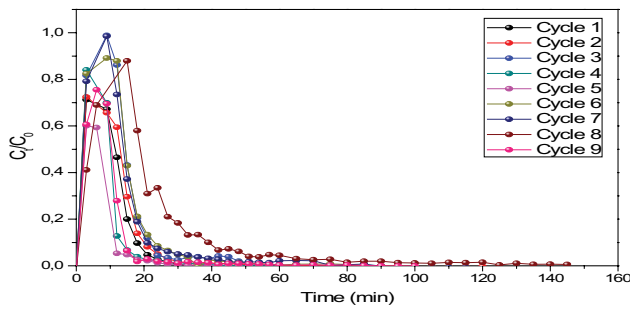


Fig. 15. Desorption of Cr(VI) using distilled water for regenerated SSS ( $F = 2 \text{ mL/min}$ ,  $Z = 20 \text{ mm}$ ,  $C_0 = 10 \text{ mg/L}$ , and  $T = 298^\circ\text{C} \pm 1^\circ\text{C}$ ).

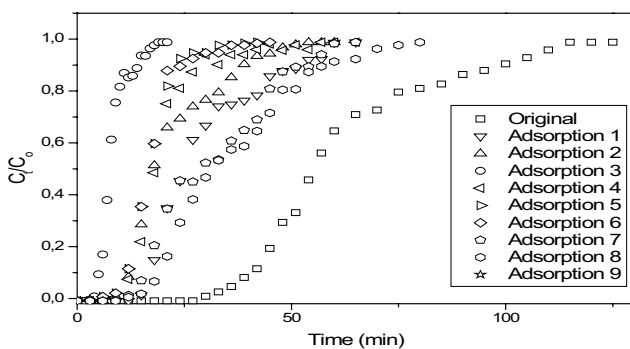


Fig. 16. Breakthrough curves for regenerated SSS ( $F = 2 \text{ mL/min}$ ,  $Z = 20 \text{ mm}$ ,  $C_0 = 10 \text{ mg/L}$ , and  $T = 298^\circ\text{C} \pm 1^\circ\text{C}$ ).

Table 5

Parameters of Thomas and Yoon and Nelson models for Cr(VI) adsorption by SSS at different conditions using non-linear regression

$C_0$ (mg/L)	$Z$ (mm)	$F$ (mL/min)	pH	$T$ (K)	Thomas model				Yoon and Nelson model			
					$K_{th} \times 10^3$ (mL/mg min)	$q_{th}$ (mg/g)	$q_{exp}$ (mg/g)	$R^2$	$K_{YN} \times 10^3$ (mL/min)	$\tau$ (min)	$\tau_{exp}$ (min)	$R^2$
10	10	2	1	298	9.69	3.06	3.42	0.9606	96.91	26.05	24	0.9606
10	20	2	1	298	9.77	3.51	3.84	0.9807	97.65	58.05	57	0.9807
10	30	2	1	298	2.55	4.92	6.08	0.9660	25.55	123.16	120	0.9660
5	20	2	1	298	8.37	2.62	2.84	0.9748	41.84	86.68	81	0.9748
15	20	2	1	298	6.26	3.56	4.00	0.9810	93.88	39.20	36	0.9810
10	20	1	1	298	3.50	3.48	4.08	0.9810	35.01	114.76	115	0.9810
10	20	3	1	298	9.57	4.36	4.74	0.9786	95.71	48.02	45	0.9786
10	20	2	2	298	8.71	1.21	1.23	0.9459	87.06	20.10	18	0.9459
10	20	2	3	298	26.35	0.32	0.26	0.8624	263.54	5.40	3	0.9852
10	20	2	1	318	4.97	3.67	4.07	0.9820	49.70	60.69	57	0.9644
10	20	2	1	308	2.40	5.96	6.22	0.9231	23.98	95.05	95	0.9231

### 5.3.7. Dynamic modeling

5.3.7.1. *Thomas and Yoon Nelson models* According to Table 5, it should be noticed that  $K_{YN}/C_0$  is equal to  $K_{th}$ , this proves that the expression of Yoon and Nelson’s solution is equivalent to Thomas’ relationship. It is also interesting to observe that the correlation coefficient  $R^2$  values for the two models Thomas and Yoon and Nelson are for the most part effects greater than 0.95 for all parameters, also the adsorption capacities and  $\tau$  values calculated by the two models and the experimental values are close enough. It is arguable that both models studied are appropriate to describe Cr(VI) adsorption.

5.3.7.2. *Bohart–Adams and Wolborska models* According to Table 6,  $\beta_a/N_0$  is equal to  $K_{BA}$ , which proves that the expression of Wolborska’s solution is equivalent to the Bohart–Adams relationship. The values of the Wolborska model’s kinetic constant are found to be influenced by all the studied parameters. This highlights that the external mass transfer into the beginning part of the sorption process dominates the system [64], The  $\beta_a$  parameter reflects the effect of mass transfer in the liquid phase and axial dispersion. An increase in flow rate from 1 to 3 mL/min enhanced the value of  $\beta_a$  because increasing turbulence reduces the boundary of the film surrounding the absorbent particle [65].  $N_0$  values were calculated by Bohart–Adams and Wolborska, and the values obtained experimentally are distant enough. Furthermore, according to the superposition of the experimental results (points) and the calculated theoretical points (lines). It seems that neither the breakthrough nor the set of failure curves are well predicted by these two models. It can be argued that both models studied are inappropriate to describe Cr(VI) adsorption.

5.3.7.3. *Model of BDST* According to Fig. 17 and Table 7, the plot of the BDST model showed significant linearity having a high value of correlation coefficient  $R^2$ , exceeded 0.90

Table 6

Parameters of Bohart–Adams and Wolborska models for Cr(VI) adsorption by SSS at different conditions using non-linear regression

Bohart–Adams model									Wolborska model			
$C_0$ (mg/L)	$Z$ (mm)	$F$ (mL/min)	pH	$T$ (K)	$K_{BA} \times 10^3$ (mL/mg min)	$N_0$ (mg/L)	$N_{exp}$ (mg/L)	$R^2$	$\beta_a$ (min <sup>-1</sup> )	$N_0$ (mg/L)	$N_{exp}$ (mg/L)	$R^2$
10	10	2	1	298	112.83	346.05	612.18	0.9894	39.04	346.05	612.18	0.9891
10	20	2	1	298	17.61	691.06	687.36	0.9850	12.82	676.50	687.36	0.9302
10	30	2	1	298	9.76	691.35	1,088.32	0.9204	46.75	691.19	1,088.32	0.9204
5	20	2	1	298	25.36	424.65	508.36	0.8979	10.77	424.60	508.36	0.9879
15	20	2	1	298	16.11	575.00	716.00	0.9595	9.26	575.02	716.00	0.9595
10	20	1	1	298	10.08	546.64	730.32	0.9655	6.28	513.93	730.32	0.9045
10	20	3	1	298	29.99	762.18	848.46	0.9936	22.99	766.51	848.46	0.9873
10	20	2	2	298	109.26	97.25	220.17	1	10.62	97.25	220.17	1
10	20	2	3	298	/	/	/	/	/	/	/	/
10	20	2	1	318	26.65	482.82	728.53	0.9372	12.87	482.75	728.53	0.9372
10	20	2	1	308	19.50	607.18	1,113.38	0.9457	11.83	607.16	1,113.38	0.9457

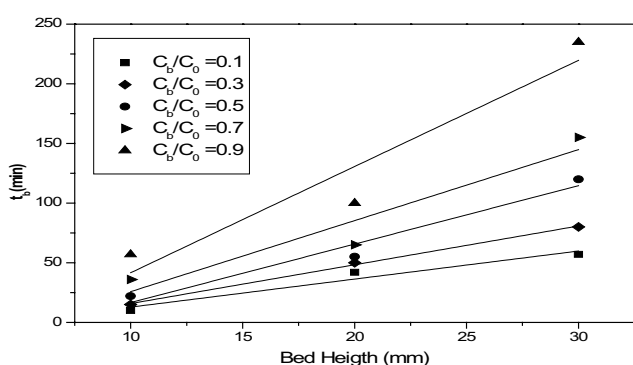


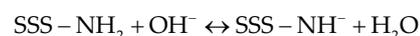
Fig. 17. Linear regression of BDST model at different breakthrough points ( $C_0 = 10$  mg/L and  $F = 2$  mL/L).

which advocated for its validity, The results found are in agreement with other studies [66,67].

## 6. Mechanism for adsorption of Cr(VI) by SSS

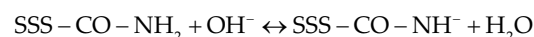
Several experimental factors, namely, the nature and complexity of the adsorbate structure, the existence of functional groups and the surface chemistry (charge, available sites) of the adsorbent, specific interactions between adsorbate and adsorbent, come into play during the adsorption process, therefore, to better understand the possible interactions, a mechanism is proposed.

Based on the results of FTIR, it can be noted that SFS contains  $-\text{COOH}$ ,  $-\text{COH}$ ,  $-\text{CO}-\text{NH}_2$ , and  $-\text{NH}_2$  functional groups.



(Amino deprotonate)

(A)



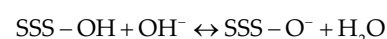
(Amino deprotonate)

(B)

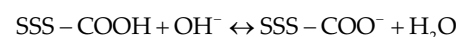
Table 7

Calculated constants of BDST model for Cr(VI) adsorption

$C_b/C_0$	$a$ (min/cm)	$b$ (min)	$K_{BA} \times 10^3$ (L/mg min)	$N'_0$ (mg/L)	$R^2$
0.1	2.35	-10.66	20.61	598.70	0.9581
0.3	3.25	-16.66	20.21	828.00	0.9980
0.5	4.90	-32.33	12.03	1,248.77	0.9656
0.7	5.95	-33.66	12.57	1,515.88	0.9194
0.9	8.90	-47.33	9.48	2,267.45	0.9182



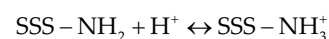
(C)



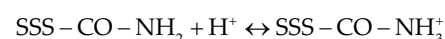
(D)

The negative charge of the polysaccharide chains resulting from deprotonation of the active sites produces an electrostatic repulsion with  $\text{HCrO}_4^-$  which inhibits the adsorption of this last one.

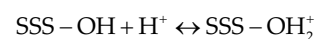
However, in the acidic medium, the functional groups amino, carboxylic, hydroxyl, and so on are protonated, and as result, its surface becomes positively charged [68–70], as can be expressed by the following reactions:



(E)



(F)



(G)



(H)

Table 8  
Comparison of efficiency rate of Cr(VI) onto various adsorbents

Adsorbents	% of Removal	References
Hydrotalcite-hydroxyapatite doped with carbon nanotubes (HT-HAp/CNT15)	76.97	[72]
Hydrotalcite-hydroxyapatite doped with carbon nanotubes (HT-HAp/CNT5)	72.85	
Hydrotalcite-hydroxyapatite (HT-HAp)	54.18	
Sewage sludge biochar supported nZVI composite	80	[74]
Scenedesmus quadricauda (microalgal biochar)	57.58	[73]
<i>Phanera vahlii</i> fruit (zinc chloride activated carbon)	63.61	[71]
Artocarpus heterophyllus peel	79.71	[15]
Eggshell membrane	88.91	[13]
Raw sunflower seed shells	66.10	Present study

Therefore, the adsorption of Cr(VI) through a biomaterial SSS could be supported by the following hypothesis: adsorption of Cr(VI) ions as  $\text{HCrO}_4^-$  on positively charged groups by electrostatic way.

It is important to compare the obtained results with the literature [71–73]. Table 7 shows a brief summary of the efficiency rate of some adsorbents for Cr(VI) removal compared with SSS powder used in this study. It is noteworthy that SSS powder has a high Cr(VI) removal efficiency compared to other adsorbents reported in the literature. This can be associated with its porous microstructure.

Meanwhile, other materials in the literature showed a high removal rate [13,15,72,74], as set out in Table 8. However, the materials reported are either fabricated from expensive components or subjected to chemical or thermal treatment (longer time and complex chemical reactions during synthesis that generally affect the purity of the final products, such as synthesis of nanoparticles, etc.

It is also important to consider other factors such as adsorbent mass, particle diameter and exhaustion, and saturation time.

## 7. Conclusion

The focus of this work was to study and model the dynamic and static removal of hexavalent chromium from aqueous solutions by sorption on the sunflower seed shells in packed bed column and batch systems.

In order to understand better the adsorptive proprieties of SSS, the material was fully characterized using different methods. Overall, the best efficiency rate was found to be 100%. Several models were applied to experimental data obtained from dynamic studies performed on fixed bed columns.

This work revealed that sunflower seed shell is an environmentally effective natural waste that can be successfully used for the removal of Cr(VI) from wastewater.

## Acknowledgments

The members acknowledge the financial support of the Algerian Ministry of Higher Education.

## Symbols

$C_0$	—	Initial Cr(VI) concentration, mg/L
$C_t$	—	Effluent Cr(VI) concentration, mg/L
$V^{\text{eff}}$	—	Effluent volume, mL
$F$	—	Influent flow rate, mL/min
$t_e$	—	Time of exhaustion, min
$t_b$	—	Time at breakthrough, min
$q_{\text{total}}$	—	Total weight of Cr(VI) adsorbed by the adsorbent in the column, mg
$q_{\text{exp}}$	—	Weight of Cr(VI) adsorbed per g of adsorbent from experiment, mg/g
$m$	—	Adsorbent mass, g
$N_{\text{exp}}$	—	Experimental maximum sorption capacity, mg/L
$V$	—	Volume of the solution, mL
$R\%$	—	Percentage of removal, %
$W_{\text{total}}$	—	Total amount of Cr(VI) sent to the column, mg
$C_{\text{ads}}$	—	Adsorbed Cr(VI) concentration, mg/L
$t$	—	Service time of the column, min
$K_{\text{th}}$	—	Kinetic constant of Thomas model, L/mg min
$q_{\text{th}}$	—	Thomas absorption capacity, mg/g
$U$	—	Linear velocity, mm/min
$K_{\text{YN}}$	—	Kinetic constant of Yoon–Nelson model, $\text{min}^{-1}$
$K_{\text{BA}}$	—	Kinetic constant of Bohart–Adams model, L/mg min
$Z$	—	Height of the bed, mm
$N_0$	—	Maximum sorption capacity, mg/L
$C_b$	—	Breakthrough concentration, mg/L
$N'_0$	—	Adsorption capacity in BDST model, mg/L
$T$	—	Temperature, °C, K
$q_e$	—	Adsorption capacity, mg/g
$q_m$	—	Maximum monolayer coverage capacity, mg/g
$K_L$	—	Langmuir constant
$K_F$	—	Freundlich isotherm constant, mg/L
$R$	—	Universal gas constant, J/K mol
$b_T$	—	Temkin isotherm constant, J/mol
$A_T$	—	Equilibrium binding constant, L/mg
$B$	—	$B = RT/b_T$ , is related to the heat of adsorption
$K_S$	—	Sips constant, $(\text{mg/L})^{-1/n}$
$q_{\text{max}}$	—	Maximum adsorption capacity, mg/g
$A$	—	Redlich–Peterson constant, L/g

## Greek

$\tau$	—	Time required for 50% adsorbate breakthrough from Yoon–Nelson model, min
$\beta_a$	—	Kinetic coefficient of the external mass transfer in the Wolborska model, min <sup>-1</sup>

## References

- [1] T.D. Ntuli, V.E. Pakade, Hexavalent chromium removal by polyacrylic acid-grafted Macadamia nutshell powder through adsorption – reduction mechanism: adsorption isotherms, kinetics and thermodynamics, *Chem. Eng. Commun.*, 207 (2019) 279–294.
- [2] Z. Chen, B. Wei, S. Yang, Q. Li, L. Liu, S. Yu, Synthesis of PANI/AIOOH composite for Cr(VI) adsorption and reduction from aqueous solutions, *ChemistrySelect*, 4 (2019) 2352–2362.
- [3] N. Abdollahi, A. Morsali, Highly sensitive fluorescent metal-organic framework as a selective sensor of Mn<sup>VII</sup> and Cr<sup>VI</sup> anions (MnO<sub>4</sub><sup>-</sup>/Cr<sub>2</sub>O<sub>7</sub><sup>2-</sup>/CrO<sub>4</sub><sup>2-</sup>) in aqueous solutions, *Anal. Chim. Acta*, 1064 (2019) 119–125.
- [4] J. Ali, L. Wang, H. Waseem, R. Djellabi, N.A. Oladoja, G. Pan, FeS@rGO nanocomposites as electrocatalysts for enhanced chromium removal and clean energy generation by microbial fuel cell, *Chem. Eng. J.*, 384 (2019) 1–29, doi: 10.1016/j.cej.2019.123335.
- [5] A. Saeedi-jurkuyeh, A.J. Jafari, R. Rezaei, A. Esrafil, A novel synthetic thin-film nanocomposite forward osmosis membrane modified by graphene oxide and polyethylene glycol for heavy metals removal from aqueous solutions, *React. Funct. Polym.*, 146 (2019) 1–56, doi: 10.1016/j.reactfunctpolym.2019.104397.
- [6] T. Shahnaz, S.M.M. Fazil, V.C. Padmanaban, S. Narayanasamy, Surface modification of nanocellulose using polypyrrole for the adsorptive removal of Congo red dye and chromium in binary mixture Tasrin, *Int. J. Biol. Macromol.*, 151 (2020) 322–332.
- [7] Y. Cao, W. Xiao, G. Shen, G. Ji, Y. Zhang, C. Gao, L. Han, Carbonization and ball milling on the enhancement of Pb(II) adsorption by wheat straw: competitive effects of ion exchange and precipitation, *Bioresour. Technol.*, 273 (2019) 70–76.
- [8] J. Xia, X. Lei, Y. Lu, S. Liu, X. Luo, Coagulation mechanism of cellulose/metal nanohybrids through a simple One-Step process and their interaction with Cr(VI), *Int. J. Biol. Macromol.*, 142 (2019) 404–411.
- [9] R. Li, D. Hu, K. Hu, H. Deng, M. Zhang, A. Wang, R. Qiu, K. Yan, Coupling adsorption-photocatalytic reduction of Cr(VI) by metal-free N-doped carbon, *Sci. Total Environ.*, 704 (2019) 1–20, doi: 10.1016/j.scitotenv.2019.135284.
- [10] R. Djellabi, L. Zhang, B. Yang, M.R. Haider, X. Zhao, Sustainable self-floating lignocellulosic biomass-TiO<sub>2</sub>@aerogel for outdoor solar photocatalytic Cr(VI) reduction, *Sep. Purif. Technol.*, 229 (2019) 1–10, doi: 10.1016/j.seppur.2019.115830.
- [11] J. Geng, Y. Yin, Q. Liang, Z. Zhu, H. Luo, Polyethyleneimine cross-linked graphene oxide for removing hazardous hexavalent chromium: adsorption performance and mechanism, *Chem. Eng. J.*, 361 (2019) 1497–1510.
- [12] Momina, M. Shahadat, S. Isamil, Regeneration performance of clay-based adsorbents for the removal of industrial dyes: a review, *RSC Adv.*, 8 (2018) 24571–24587.
- [13] A. Lahmar, Z. Hattab, R. Zerdoum, N. Boutemine, R. Djellabi, Dynamic sorption of hexavalent chromium using sustainable low-cost eggshell membrane, *Desal. Water Treat.*, 181 (2020) 289–299.
- [14] E. Nakkeeran, C. Patra, T. Shahnaz, S. Rangabhashiyam, N. Selvaraju, Continuous biosorption assessment for the removal of hexavalent chromium from aqueous solutions using *Strychnos nux vomica* fruit shell, *Bioresour. Technol. Rep.*, 3 (2018) 256–260.
- [15] N. Saranya, A. Ajmani, V. Sivasubramanian, N. Selvaraju, Hexavalent chromium removal from simulated and real effluents using *Artocarpus heterophyllus* peel biosorbent - batch and continuous studies, *J. Mol. Liq.*, 265 (2018) 779–790.
- [16] R. Djellabi, B. Yang, H.M. Adeel Sharif, J. Zhang, J. Ali, X. Zhao, Sustainable and easy recoverable magnetic TiO<sub>2</sub>-Lignocellulosic Biomass@Fe<sub>3</sub>O<sub>4</sub> for solar photocatalytic water remediation, *J. Cleaner Prod.*, 233 (2019) 841–847.
- [17] R. Djellabi, B. Yang, Y. Wang, X. Cui, X. Zhao, Carbonaceous biomass-titania composites with Ti–O–C bonding bridge for efficient photocatalytic reduction of Cr(VI) under narrow visible light, *Chem. Eng. J.*, 366 (2019) 172–180.
- [18] B. Kocadagistan, E. Kocadagistan, The effects of sunflower seed shell modifying process on textile dye adsorption : kinetic, thermodynamic and equilibrium study, *Desal. Water Treat.*, 57 (2016) 3168–3178.
- [19] S. Alizadeh, K. Seyyedi, Removal of C.I. Acid red 1 (AR1) dye pollutant from contaminated waters by adsorption method using sunflower seed shells and pine cone as agro-waste materials, *Appl. Chem. Res.*, 13 (2019) 93–105.
- [20] A. Truskewycz, M. Taha, D. Jampaiah, R. Shukla, A.S. Ball, I. Cole, Interfacial separation of concentrated dye mixtures from solution with environmentally compatible nitrogenous-silane nanoparticles modified with *Helianthus annuus* husk extract, *J. Colloid Interface Sci.*, 560 (2020) 825–837.
- [21] M.E. Saleh, A.A. El-refaey, A.H. Mahmoud, Effectiveness of sunflower seed husk biochar for removing copper ions from wastewater: a comparative study, *Soil Water Res.*, 11 (2016) 53–63.
- [22] S. Srisorrachatr, Modified sunflower seed husks for metal ions removal from wastewater, *Chem. Eng. Trans.*, 57 (2017) 247–252.
- [23] W. Srisuwan, C. Jubsilp, S. Srisorrachatr, The use of K<sub>2</sub>CO<sub>3</sub> modified sunflower seed husks for removing of metal ions from industrial wastewater, *Chem. Eng. Trans.*, 70 (2018) 241–246.
- [24] S.A. Abdulhusein, A.I. Al wared, Single and binary adsorption of Cu(II) and Ni(II) ions from aqueous solutions by sunflower seed husk, *Assoc. Arab Univ. J. Eng. Sci.*, 26 (2019) 35–43.
- [25] S. Zhang, X. Yang, M. Ju, L. Liu, K. Zheng, Mercury adsorption to aged biochar and its management in China, *Environ. Sci. Pollut. Res.*, 26 (2018) 4867–4877.
- [26] S. Stanković, T. Soštarić, M. Bugarčić, A. Janičević, K. Pantović-Spajić, Z. Lopičić, Adsorption of Cu(II) ions from synthetic solution by sunflower seed husks, *Acta Period. Technol.*, 50 (2019) 268–277.
- [27] M. Jain, V.K. Garg, R. Paliwal, K. Kadirvelu, S. Chaudhry, Optimization of cadmium(II) removal from water using sunflower waste carbon—a statistical approach, *Toxin Rev.*, (2020) 1–10, doi: 10.1080/15569543.2020.1718163.
- [28] B. Hayoun, M. Bourouina, M. Pazos, M.A. Sanromán, S. Bourouina-Bacha, Equilibrium study, modeling and optimization of model drug adsorption process by sunflower seed shells, *Appl. Sci.* 10 (2020) 3271, doi: 10.3390/app10093271.
- [29] F. Zohra, S. Hazourli, S. Nouacer, H. Rahima, Valorization of raw biomaterial waste-date stones-for Cr(VI) adsorption in aqueous solution: thermodynamics, kinetics and regeneration studies, *Int. Biodeterior. Biodegrad.*, 114 (2016) 76–86.
- [30] I. Langmuir, The constitution and fundamental properties of solids and liquids. Part II.-Liquids, *J. Franklin Inst.*, 184 (1917) 721.
- [31] H.M.F. Freundlich, Over the adsorption in solution, *J. Phys. Chem.*, 57 (1906) 385–471.
- [32] V. Temkin, M.I. Pyzhev, Kinetics of ammonia synthesis on promoted iron catalyst, *Acta Phys. Chim.*, 12 (1940) 217–222.
- [33] N. Ayawei, A.N. Ebelegi, D. Wankasi, Modelling and interpretation of adsorption isotherms, 2017 (2017) 1–11, doi: 10.1155/2017/3039817.
- [34] R. Sips, On the structure of a catalyst surface, *J. Chem. Phys.*, 16 (1948) 490–495.
- [35] M. Saxena, N. Sharma, R. Saxena, Highly efficient and rapid removal of a toxic dye: adsorption kinetics, isotherm, and mechanism studies on functionalized multiwalled carbon nanotubes, *Surf. Interfaces*, 21 (2020) 1–10, doi: 10.1016/j.surfint.2020.100639.

- [36] M.A. Al-Ghouti, D.A. Da'ana, Guidelines for the use and interpretation of adsorption isotherm models: a review, *J. Hazard. Mater.*, 393 (2020) 1–22, doi: 10.1016/j.jhazmat.2020.122383.
- [37] J. Rodier, B. Legube, N. Merlet, *L'Analyse de L'eau*, 9th ed., DUNOD, Paris, 2009.
- [38] M. Basu, A.K. Guha, L. Ray, Adsorption of cadmium ions by cucumber peel in continuous mode, *Int. J. Environ. Sci. Technol.*, 16 (2019) 237–248.
- [39] M.E. González-López, A.A. Pérez-Fonseca, M. Arellano, C. Gómez, J.R. Robledo-Ortiz, Fixed-bed adsorption of Cr(VI) onto chitosan supported on highly porous composites, *Environ. Technol. Innovation*, 19 (2020) 1–9, doi: 10.1016/j.eti.2020.100824.
- [40] S. Charola, R. Yadav, P. Das, S. Maiti, Fixed-bed adsorption of Reactive Orange 84 dye onto activated carbon prepared from empty cotton flower agro-waste, *Sustainable Environ. Res.*, 28 (2018) 298–308.
- [41] J. López-Cervantes, D.I. Sánchez-Machado, R.G. Sánchez-Duarte, M.A. Correa-Murrieta, Study of a fixed-bed column in the adsorption of an azo dye from an aqueous medium using a chitosan–glutaraldehyde biosorbent, *Adsorpt. Sci. Technol.*, 36 (2018) 215–232.
- [42] H.A. Alalwan, M.N. Abbas, Z.N. Abudi, Environmental technology & innovation adsorption of thallium ion (Tl<sup>3+</sup>) from aqueous solutions by rice husk in a fixed-bed column: experiment and prediction of breakthrough curves, *Environ. Technol. Innovation*, 12 (2018) 1–13.
- [43] A.R. Gouran-orimi, B. Mirzayi, Competitive adsorption of nitrate in fixed-bed column packed with bio-inspired polydopamine coated zeolite, *Environ. Chem. Eng.*, 6 (2018) 2232–2240.
- [44] H.C. Thomas, Heterogeneous ion exchange in a flowing system, *J. Am. Chem. Soc.*, 66 (1944) 1664–1666.
- [45] Y.H. Yoon, J.H. Nelson, Application of gas adsorption kinetics I. A theoretical model for respirator cartridge service life, *Am. Ind. Hyg. Assoc. J.*, 45 (1984) 509–516.
- [46] G.S. Bohart, E.Q. Adams, Some aspects of the behaviour of charcoal with respect to chlorine, *J. Am. Chem. Soc.*, 42 (1920) 523–544.
- [47] A. Wolborska, Adsorption on activated carbon of p-nitrophenol from aqueous solution, *Water Res.*, 23 (1989) 85–91.
- [48] P. Arromdee, V.I. Kuprianov, A comparative study on combustion of sunflower shells in bubbling and swirling fluidized-bed combustors with a cone-shaped bed, *Chem. Eng. Process. Process Intensif.*, 62 (2012) 26–38.
- [49] J. Choi, B. Pant, C. Lee, M. Park, S.J. Park, H.Y. Kim, Preparation and characterization of eggshell membrane/PVA hydrogel via electron beam irradiation technique, *J. Ind. Eng. Chem.*, 47 (2017) 41–45.
- [50] N. Quaranta, M. Caligaris, G. Pelozo, A. Césari, A. Cristóbal, Use of wastes from the peanut industry in the manufacture of building materials, *Int. J. Sustainable Dev. Plann.*, 13 (2018) 662–670.
- [51] A. Hadfi, S. Ben Aazza, M. Belattar, S. Mohareb, A. Driouiche, Evaluation of the irrigation water quality in Biougra circle along with highlighting the effectiveness of a scaling inhibitor, *Mediterr. J. Chem.*, 7 (2018) 272–285.
- [52] S. Park, K.S. Choi, D. Lee, D. Kim, K.T. Lim, K.H. Lee, H. Seonwoo, J. Kim, Eggshell membrane: review and impact on engineering, *Biosyst. Eng.*, 151 (2016) 446–463.
- [53] E. Bilgic, S. Yaman, S. Kucukbayrak, Limits of variations on the structure and the fuel characteristics of sun flower seed shell through torrefaction, *Fuel Process. Technol.*, 144 (2016) 197–202.
- [54] R.M. Ali, H.A. Hamad, M.M. Hussein, G.F. Malash, Potential of using green adsorbent of heavy metal removal from aqueous solutions: adsorption kinetics, isotherm, thermodynamic, mechanism and economic analysis, *Ecol. Eng.*, 91 (2016) 317–332.
- [55] R. Djomi, L.J.R. Meva'a, J. Nganhou, G. Mbobda, A.E. Njom, Y.D.M. Bampel, J.-B.S. Tchinda, Physicochemical and thermal characterization of dura palm kernel powder as a load for polymers: case of polyvinyl chloride, *J. Mater. Sci. Chem. Eng.*, 6 (2018) 1–18.
- [56] A. Bala-Litwiniak, M. Zajemska, Computational and experimental study of pine and sunflower husk pellet combustion and co-combustion with oats in domestic boiler, *Renewable Energy*, 162 (2020) 151–159.
- [57] D. Cherek, K. Louhab, Kinetics, isotherms, and thermodynamic study of diclofenac adsorption using activated carbon prepared from olive stones, *J. Dispersion Sci. Technol.*, 39 (2018) 814–825.
- [58] R. Totani, C. Méthivier, D. Costa, T. Jaffrelot Inizan, C.M. Pradier, V. Humblot, Binding and 2D organization of arginine on Cu(1 1 0), *Appl. Surf. Sci.*, 509 (2020) 1–8.
- [59] H. Yanagisawa, Y. Matsumoto, M. Machida, Adsorption of Zn(II) and Cd(II) ions onto magnesium and activated carbon composite in aqueous solution, *Appl. Surf. Sci.*, 256 (2010) 1619–1623.
- [60] M.J. Ahmed, B.H. Hameed, Ecotoxicology and environmental safety removal of emerging pharmaceutical contaminants by adsorption in a fixed-bed column: a review, *Ecotoxicol. Environ. Saf.*, 149 (2018) 257–266.
- [61] D.S.P. Franco, J.L.S. Fagundes, J. Georjina, N. Paula, G. Salau, A mass transfer study considering intraparticle diffusion and axial dispersion for fixed-bed adsorption of crystal violet on pecan pericarp (*Carya illinoensis*), *Chem. Eng. J.*, 397 (2020) 1–9, doi: 10.1016/j.cej.2020.125423.
- [62] R. Jobby, P. Jha, A.K. Yadav, N. Desai, Biosorption and biotransformation of hexavalent chromium [Cr(VI)]: a comprehensive review, *Chemosphere*, 207 (2018) 255–266.
- [63] M. Jain, V. Kumar, K. Kadirvelu, Adsorption of hexavalent chromium from aqueous medium onto carbonaceous adsorbents prepared from waste biomass, *J. Environ. Manage.*, 91 (2010) 949–957.
- [64] R. Zerdoum, Z. Hattab, Y. Berredjem, R. Mazouz, Removal of methylene blue from water using eggshell membrane fixed bed, *Desal. Water Treat.*, 81 (2017) 252–264.
- [65] N. Singh, C. Balomajumder, Continuous packed bed adsorption of phenol and cyanide onto modified rice husk: an experimental and modeling study, *Desal. Water Treat.*, 57 (2016) 23903–23917.
- [66] M. Talata, S. Mohan, V. Dixit, D.K. Singh, S.H. Hasan, O.N. Srivastava, Effective removal of fluoride from water by coconut husk activated carbon in fixed bed column: experimental and breakthrough curves analysis, *Groundwater Sustainable Dev.*, 7 (2018) 48–55.
- [67] S. Aydın, A. Traore, E. Yıldırım, H. Mowlid Nur, S. Emik, Fixed bed column adsorption of vanadium from water using amino-functional polymeric adsorbent, *Desal. Water Treat.*, 209 (2021) 280–288.
- [68] C. Manera, A.P. Tonello, D. Perondi, Adsorption of leather dyes on activated carbon from leather shaving wastes: kinetics, equilibrium and thermodynamics studies, *Environ. Technol.*, 40 (2018) 2756–2768.
- [69] W. Bessashia, Y. Berredjem, Z. Hattab, M. Bououdina, Removal of basic fuchsin from water by using mussel powdered eggshell membrane as novel bioadsorbent: equilibrium, kinetics, and thermodynamic studies, *Environ. Res.*, 186 (2020) 1–12, doi: 10.1016/j.envres.2020.109484.
- [70] T. Józwiak, U. Filipkowska, S. Brym, L. Kopeć, Use of aminated hulls of sunflower seeds for the removal of anionic dyes from aqueous solutions, *Int. J. Environ. Sci. Technol.*, 17 (2020) 1211–1224.
- [71] A. Ajmani, C. Patra, S. Subbiah, S. Narayanasamy, Packed bed column studies of hexavalent chromium adsorption by zinc chloride activated carbon synthesized from *Phanera vahlii* fruit biomass, *J. Environ. Chem. Eng.*, 8 (2020) 1–7, doi: 10.1016/j.jece.2020.103825.
- [72] E. Rodrigues, O. Almeida, H. Brasil, D. Moraes, M.A.L. dos Reis, Adsorption of chromium(VI) on hydroxylated hydroxyapatite material doped with carbon nanotubes: equilibrium, kinetic and thermodynamic study, *Appl. Clay Sci.*, 172 (2019) 57–64.

- [73] E. Daneshvar, M.J. Zarrinmehr, M. Kousha, A.M. Hashtjin, G.D. Saratale, A. Maiti, M. Vithanage, A. Bhatnagar, Hexavalent chromium removal from water by microalgal-based materials: adsorption, desorption and recovery studies, *Bioresour. Technol.*, 293 (2019) 1–8, doi: 10.1016/j.biortech.2019.122064.
- [74] Z. Fan, Q. Zhang, B. Gao, M. Li, C. Liu, Y. Qiu, Removal of hexavalent chromium by biochar supported nZVI composite: batch and fixed-bed column evaluations, mechanisms, and secondary contamination prevention, *Chemosphere*, 217 (2019) 85–94.